Granular dynamics in a swirled annulus

Michael A. Scherer,[1] Thomas Mahr,[1] Andreas Engel,[2] and Ingo Rehberg[1]
[1]*Institut für Experimentelle Physik, Otto-von-Guericke-Universität, Postfach 4120, D-39016 Magdeburg, Germany*
[2]*Institut für Theoretische Physik, Otto-von-Guericke-Universität, Postfach 4120, D-39016 Magdeburg, Germany*
(Received 29 July 1997; revised manuscript received 22 May 1998)

A swirled annular channel is introduced that is suited to study the dynamics of granular arrays. We uncover the mechanism that is responsible for the change of the sense of rotation of a two-dimensional cluster of spheres that is excited by horizontal, orbital shaking. Experimental investigations are presented that show the influence of packing density, channel width, driving frequency, and material parameters. We compare this with a simple one-dimensional model. It is seen that the system is governed by single binary collisions that give rise to global behavior, namely, a corotating or counterrotating motion of the cluster. [S1063-651X(98)11910-4]

PACS number(s): 81.05.Rm, 83.10.Pp

I. INTRODUCTION

Recently it was stated that granular material should be considered as an additional state of matter in its own right [1]. Shaking sand, mixing cereals, or smashing frozen tomatoes exhibit phenomena that cannot be explained by the physics of solids, liquids, or gases. A granular system might show a solidlike behavior as in the case of a simple sand pile. But it breaks down when, for example, blowing wind forces desert sand to form unique patterns of ripples and dunes. It seems to be promising to formulate a theory that is a synthesis of well established concepts: the base of a dune a solid, the surface of the ripples a fluid, and the saltated grains a simple gas. Unfortunately there was no success in establishing such a unified theory of granular matter. Nonetheless different approaches were introduced to explain the strange common behavior of grains and spheres. Computational effort started at the basics and modeled single grains and their collision dynamics [2], classical systems like Taylor-Couette devices were stressed to reveal the underlying mechanism [3] and hydrodynamical descriptions were introduced to study simple one-dimensional cases [4]. In addition to these valuable insights new surprising phenomena like ''oscillons'' [5] or ''inelastic collapse'' [6] were found that even enhance the interest we already attribute to granular material.

In this paper we study a system that is marked by its simplicity. It was shown that when spheres are placed in a circular container and experience an orbital shaking the sense of rotation of the cluster depends on the number of spheres: At low packing density, the spheres rotate in a positive direction (rotation mode) whereas at high packing densities they go the other way around (reptation mode) [7]. Because in the reptation mode the diffusion coefficient is low, i.e., the spheres barely separate, the following question arose: Is it possible to neglect the inner cluster and replace it by a fixed disk? In order to answer this question we develop a setup that consists of an annular channel where the dynamics of spheres is studied. To our surprise the same phenomenon is observed. The circular granular array changes its sense of rotation when the particles exceed a critical number.

It is found that an annular system exhibits several advantages: First, in a narrow channel the spheres cannot pass; the position of a single sphere is fixed in relation to its neighbors and can be labeled. This improves experimental techniques, such as visualization of particle trajectories, because their center of mass can be studied on a circular line.

Second, this system is suited to study related areas, namely, collision dynamics, and cluster formation. Recently there was much effort to improve the model of binary collisions [8]. Numerical simulations like molecular dynamics techniques or event driven codes rely on an almost perfect description of the collision events. To describe dissipation by a coefficient of restitution gives only a simplified picture of the impact. Classical methods such as Hertz's contact law have to be extended to achieve agreement between simulations and experimental findings [9]. Recently the concept of inelastic collapse, where particles collide infinitely often in a finite time and build clusters, caused much excitement in the field of granular material [10]. Grossman and Mungan [11] studied the motion of three particles on a ring that has an attractive similarity to our system. In the meantime investigations on the inelastic collapse of rotating spheres [12] were established. These results also fit into our schema because we do not suppress the spinning motion of the spheres. Experimental work on cluster formation already exists but without evidence of inelastic collapse [13]. We also think that our work is related to studies of one-dimensional granular columns, which deal with friction-induced self-organization [14], investigations where the particles are excited by white noise [15] or experiments where a type of solitary wave is observed [16].

Finally it is important to note that the main advantage of our simple setup is that it can be described by a one-dimensional model. Here, the spheres are one-dimensional particles with a certain length. Their centers of mass are restricted to a circular line where it is excited by a sinusoidal force that exactly simulates the conditions of our system. It is seen that this model is in good agreement with our experimental findings and that it reveals the main mechanism of the phenomenon.

This paper is arranged as follows: First we introduce our setup and present our experimental results. We study the influence of packing density, channel width, and driving frequency and we visualize the particle dynamics. In the second part we discuss this in light of a one-dimensional theoretical model. We first derive the dynamics of a single sphere. Then

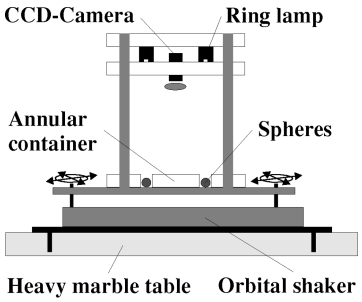

FIG. 1. Experimental setup.

we extend the model and show that the change of the sense of rotation is due to what we call ''free path restriction.'' Finally we support this picture by simulating the situation where many particles are involved.

II. EXPERIMENT

A. Experimental setup

The heart of the experimental setup, which is seen in Fig. 1, is an adjustable reciprocating orbital shaker (Thermolyne AROS 160). This device operates such that during one oscillation period every point (x,y) on the table moves in a circle in the laboratory frame according to $x=A\sin(\omega t)$ and $y=A\cos(\omega t)$, where A is the amplitude of motion, $\omega=2\pi f_d$, and f_d the driving frequency of the shaker. It is important to note that this circular motion has no center of rotation, i.e., every particle feels the same amount of centrifugal acceleration $a=\omega^2 A$. Moreover the direction of the acceleration is the same for every point. The shaker is fixed on a heavy marble table to avoid internal vibrations of the setup. The marble table weighs about 350 kg. Due to mechanical constraints f_d cannot exceed 4.5 Hz. We keep the amplitude of motion constant at $A=9.53$ mm. An annular container is fastened on the swirling table to investigate the granular dynamics of the spheres. The annulus is milled out of Plexiglas. Its outer radius R_{out} is 50 mm. The width of the channel w varies. We use six different containers with $w=10.5$, 11, 12, 14, 16, and 18 mm. The height of the channel is 10 mm. To characterize the surface of the annular channel we measured the arithmetic average roughness R_a and the total roughness R_t of the annulus. We used a surface analyzer (Talysurf Serie 120) with a resolution of 32.0 nm. We determined the surface roughness along a width of 10 mm at three different points of the channel which resulted in $R_a=2.80$ μm and $R_t=15.60$ μm, respectively. A charge-coupled device (CCD) camera is mounted on top of the swirling table to take images for analysis in the comoving frame. For visualization of the particle trajectories an annular lamp (Schott KL 1500 electronic) on top of the setup is used. As spheres we use precision beads of five different materials: bronze (material density $\rho=8.5$ g/cm^3), brass (8.4 g/cm^3), Polyurethane (PUR) (1.2 g/cm^3), an elastomer, and two types of soda lime glass (glass) (2.5 g/cm^3) spheres, one with a rough surface and the other with a polished surface. The sphere diameter d is the same for all materials, 10 mm. However, tolerances of the diameter differ: bronze and brass, ± 0.11 mm; PUR, -0.15 to $+0.10$ mm; and Soda Lime glass, ± 0.02 mm.

B. Experimental results

To exhibit the effect that granular material swirled in a circular container changes its sense of rotation when the packing density is increased we perform four different sets of experiments. First we show that the effect is robust and can be restricted to a narrow annulus where neighboring spheres cannot pass. Hence the problem is reduced to a one-dimensional array where the granular column is allowed to move on a circle that has periodic boundary conditions. Second we show the influence of the channel width to obtain information on the dynamical behavior of the spheres for the transition from open container to narrow channel. Moreover we change the driving frequency of the system. These results are shown in the third section for different materials. Finally we try to track down the essence of the mechanism by visualizing the particle trajectories.

1. Influence of packing density

In the first experiment we capture the basic features of the effect that granular material changes from a rotation to a reptation mode when the number of particles N is increased. Here we choose a channel with the smallest width, 10.5 mm. This means that the spheres have clearance of about 0.25 mm on each side. The driving frequency is set to 2.5 Hz. The spheres are made of bronze. We measure the time T_s a single sphere needs to orbit the whole channel. This period of rotation is measured five times. It is seen that this value sensitively depends on the horizontal alignment of the container. If the annulus is slightly tilted the sphere velocities vary in different sections of the channel. In addition, due to inhomogeneities of the channel width this effect is enhanced. To ensure that the velocities are almost homogeneously distributed we test the speed of a single sphere by the following procedure: We divide the annulus into four quarters and measure the time the bead needs to pass a certain section. We adjust the channel in such a way that these times only differ by $\pm 15\%$.

To obtain the phase diagram we start with one particle and increase the packing density in steps of one particle number. At a minimum, we wait 2 min until the velocities adjust. At the critical point this time has to be increased because the cluster moves very slowly. We wait at least until the measured times are almost constant, which is about five times T_s. The results are seen in Fig. 2. We also plot the standard deviation as bars. The period of rotation is almost constant at about 25 s while no collisions occur, i.e., for $N=1,\ldots,15$. If the particle number is larger than 15, neighboring spheres tend to collide. This is simply noted by sound emission. At this stage the spheres slow down. For 21 particles the period of rotation is about three times higher than for noncolliding particles. At particle number 22 the sense of rotation of the cluster changes its sign and rotates the other way around. This is what we describe as the reptation mode [7]. Further increase of N increases the particle velocities. Nevertheless this behavior breaks down for 27 and 28 particles. Here, packing density is so high that again the cluster slows down.

For $N=24$ we observe a longitudinal density wave (LDW). A snapshot of the setup under this condition shows that the spheres are not homogeneously distributed. The packing density is high in the region where two spheres col-

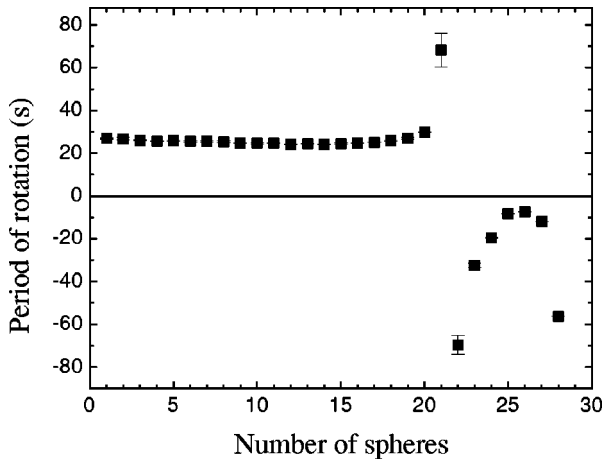

FIG. 2. Dependence of the period of rotation on the number of spheres (material: bronze; channel width: 10.5 mm; driving frequency: 2.5 Hz).

lide and low on the opposite side of the channel. The region of maximum packing density, namely, the collision point of two spheres, circulates in the positive direction with the same frequency as the driving frequency of the swirling table and resembles a solitary density wave. LDWs are also found for $N=21$, 22, and 23. However, here the wave extinguishes because of voids where the particle density is too low and a binary collision cannot occur because the spheres do not touch. However, it will again start if the particle density becomes sufficiently high.

2. Influence of channel width

To study the influence of the channel width w we conduct the same experiment as described in the preceding section but using different channels. Again we use bronze spheres. The driving frequency is now fixed at 3 Hz. Figure 3 shows results for $w=10.5$ mm and 18.0 mm, respectively. In this diagram we plot the frequency of rotation f_s of the cluster instead of the period of rotation T_s as in Fig. 2. Therefore the critical point N_c is not a singularity; it is now located where the curve intersects $f_s=0$. Because our particles are discrete we cannot exactly measure N_c. Moreover, near the critical

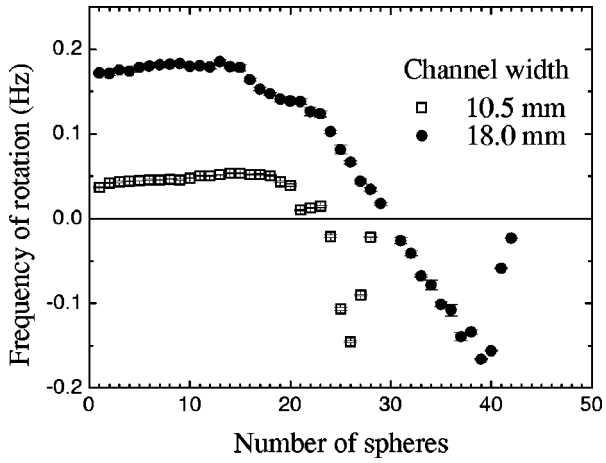

FIG. 3. Dependence of the frequency of rotation on the number of spheres for two different channel widths (material: bronze; driving frequency: 3 Hz).

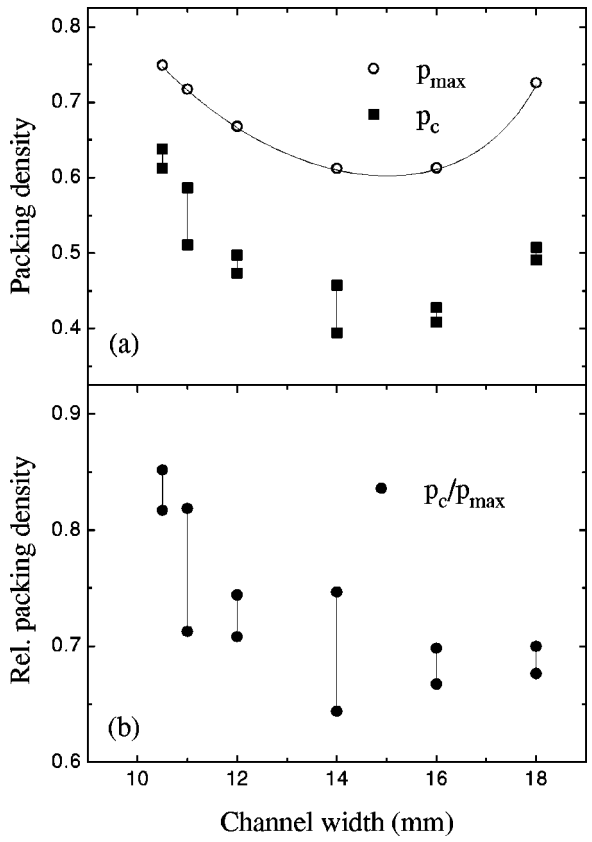

FIG. 4. (a) Influence of the channel width on the critical packing density p_c of the spheres and the maximum packing density $p_{\max}$. (b) Relative packing density $p_c/p_{\max}$ with respect to the channel width (material: bronze; driving frequency: 3 Hz).

point the cluster is sometimes so slow that we cannot obtain any measurement within a reasonable time. However, in this case we can determine a lower and upper boundary for the particle number where the change of the sense of rotation takes place. It is observed that N_c is shifted from a critical number between 23 and 24 spheres for the smallest channel to about 30 spheres for the broadest one.

To analyze the influence of the channel width on the critical point we introduce a two-dimensional critical packing density p_c. We plot the ratio of the area the spheres cover to the area of the annulus:

$$p_c=\frac{d^2N_c}{8R_{\text{out}}w-4w^2} \tag{1}$$

versus the channel width [see Fig. 4(a)]. Here we show the borders where we still observe motion of the cluster in the rotation (lower quadratic points) and reptation mode (upper quadratic points). p_c is located within this interval (bars). It is seen that $p_c(w)$ has a parabolic shape with a minimum at about $w=15$ mm. This can be related to the maximum number of spheres that fit in the annular channel and that give a maximum packing density $p_{\max}$. Its dependency on w is also shown in Fig. 4(a) (open circles).

Figure 5 serves to illustrate the determination of $p_{\max}$: If the channel is narrow and the spheres build a one-dimensional array the voids are small and thus we get a high packing density. If the channel is wide as shown in our

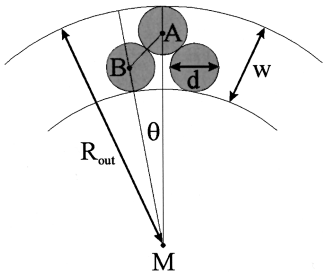

FIG. 5. Schema to calculate the dependence of the critical packing density on the channel width.

schema the center of mass of the beads arrange in a zigzag line. Because here the voids are large we get a lower packing density. The maximum packing density is derived by considering the two-dimensional area one sphere covers A_{sp} in a certain section of the channel A_{ch}. A_{ch} is determined by the angle θ.

For the following calculation we impose two constraints: First we have to take into account that the calculation is restricted to a certain range of the particle diameter: $d = 10$ mm$\leqslant w \leqslant d(1+\sqrt{3}/2) = 18.7$ mm. The upper limit refers to the case where the center of three neighboring spheres forms an equilateral triangle to achieve a close packed structure. For wider channels the spheres can be arranged in different configurations, which give different packing densities. In the experiment we do not investigate the case of $w \geqslant 18$ mm. Second the calculation only holds for $2\pi/\theta =$ integer. Nevertheless, because $\theta \ll 2\pi$ the violation of this assumption does not play a crucial role.

The maximum packing density is defined as

$$p_{\max} = \frac{A_{sp}}{A_{ch}} \tag{2}$$

with $A_{sp} = d^2\pi/4$ and $A_{ch} = (R_{out}w - w^2/2)\theta$. The only unknown value is the angle θ which can be obtained via the cosine law (see Fig. 5):

$$\overline{AB^2} = \overline{MA^2} + \overline{MB^2} - 2\overline{MA}\,\overline{MB}\cos\theta, \tag{3}$$

where $\overline{AB} = d$, $\overline{MA} = R_{out} - d/2$, and $\overline{MB} = R_{out} + d/2 - w$.

Thus,

$$\theta = \arccos\left(1 - \frac{2dw - w^2}{2R_{out}^2 - 2R_{out}w - d^2/2 + dw}\right) \tag{4}$$

and

$$p_{\max} = \frac{d^2\pi}{4R_{out}w - 2w^2} \times \left[\arccos\left(1 - \frac{2dw - w^2}{2R_{out}^2 - 2R_{out}w - d^2/2 + dw}\right)\right]^{-1}. \tag{5}$$

In Fig. 4(a) this function is shown as a curve (solid line) intersecting the open circles which denotes the maximum packing density for the examined channels. On first sight p_c looks qualitatively like $p_{\max}$ disregarding a vertical shift. The ratio $p_c/p_{\max}$, however [see Fig. 4(b)], is constant for wider channels ($w = 14$, 16, and 18 mm). For smaller channels ($w = 10.5$, 11, and 12 mm) $p_c/p_{\max}$ deviates. Nevertheless we conclude that the critical point where there is a transition from rotation to reptation mode can be related to the maximum numbers of spheres that fit into the annular channel. This is supported by the fact that the packing density rises when collisions occur as in the case of LDWs. It is likely that then the spheres almost reach the state of the highest possible packing density and that this state governs the global behavior of the cluster. We believe that this is of interest because in other systems the maximum packing density normally depends on the size distribution of the particles or on the history of achieving a packing structure [17].

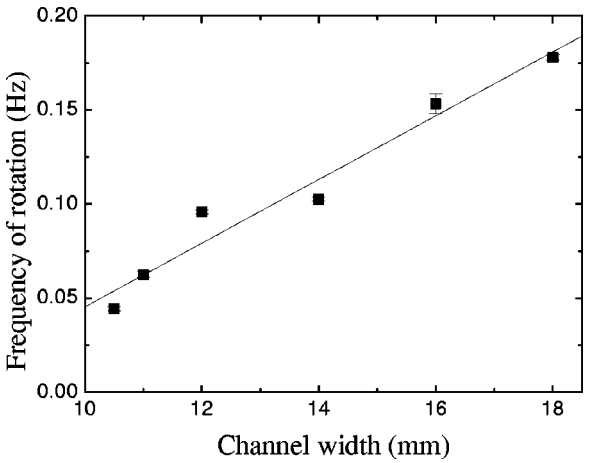

FIG. 6. Influence of the channel width on the frequency of rotation averaged for particle number 1 to 10 (material: bronze; driving frequency: 3 Hz).

Finally, our interest focuses on the influence of the channel width in the zone where no collisions are observed. Figure 3 shows that in this region N has no influence on f_s. The resulting plateau is a characteristic feature of the phase diagram. We derive the mean value of the rotation frequency for beads 1 to 10 and show it versus the channel width (Fig. 6). A linear dependency is obtained. Because the probability of sphere-wall collisions is less in the wider channel the spheres have a better chance of gaining a larger velocity before colliding with the walls. This is of importance for obtaining a one-dimensional theory of the problem, because it cannot take into account the clearance of the spheres. Extrapolating the line in Fig. 6 to $w = 10$ mm, which is the sphere diameter, hints at how the dynamics of a single sphere in the no-collision zone has to be modeled.

3. Influence of driving frequency

In this section we look at the dependence of the rotation frequency of the cluster on the driving frequency of our system. We restrict our measurements to the channel width $w = 10.5$ mm and use bronze spheres. Figure 7 shows results for different particle numbers. For 1 and 10 particles the response of f_s on f_d is linear, neglecting the initial points at $f_d = 1$ Hz. For $N = 20$ we find a quite similar behavior, but at high frequencies ($f_d \geqslant 3.5$ Hz) we approach a new regime: Here we notice the onset of LDWs, which result in a

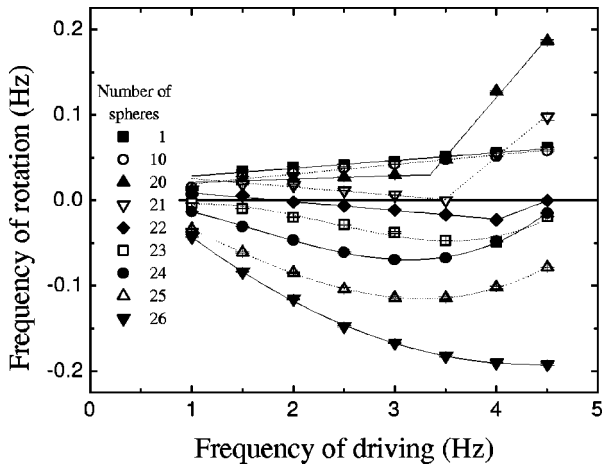

FIG. 7. Dependence of the frequency of rotation of the spheres on the driving frequency of the swirling table for different numbers of spheres (material: bronze; channel width: 10.5 mm).

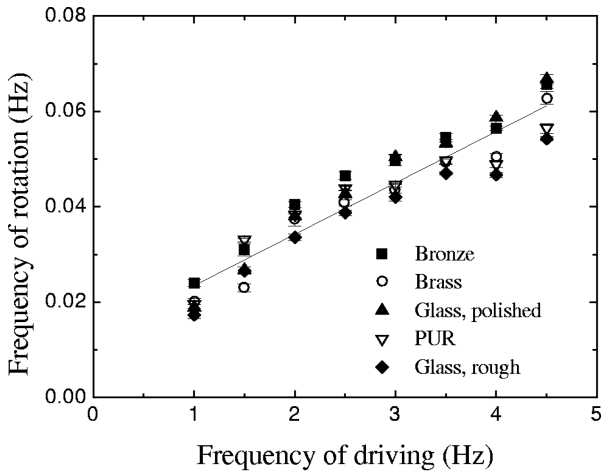

FIG. 8. Dependence of the frequency of rotation on the driving frequency for different materials (number of spheres: 10; channel width: 10.5 mm). The line serves as a guide to the eye.

higher velocity of the spheres. This onset is also observed for 20 and 21 spheres although at higher driving frequencies. For $N=22$ we observe that f_d changes its sign, i.e., that the cluster reptates at low frequencies and rotates at high frequencies. Thus, we conclude that the critical point where the sense of rotation changes not only depends on the packing density but also on the driving frequency. 24, 25, and 26 spheres show that f_s first increases as f_d is increased but also that the spheres slow down at high frequencies. For these particle numbers the curves in Fig. 7 are obtained by parabolic fits and serve as a guide to the eye. We believe that the velocity reduction at high driving frequencies is due to the fact that the dynamics of a single sphere is different in this regime. Here the friction coefficient between sphere material and Plexiglas might change, or the spinning motion of the spheres might become significant. That this is of importance can be experienced during every billiard game [18] and was also observed by Drake performing granular flow experiments [19]. By visual inspection we observe that the spheres are more likely to slide at high frequencies and high packing densities. This can be explained by the fact that after a collision a sphere has a higher velocity compared to the situation at low frequencies and low packing densities. According to Ref. [20] the transition time from sliding to rolling for a single sphere depends linearly on the velocity. Nevertheless this phenomenon remains to be understood. Further investigations with high speed visualization and a technique that allows resolution of the spin of a single sphere are necessary to uncover the underlying mechanism.

In addition we study the response behavior of different materials. Under the above-mentioned conditions we perform runs with five different materials: bronze, brass, PUR, glass (polished and rough). In Fig. 8 we see the behavior of a cluster of 10 particles. It is seen that there is only a slight discrepancy for different materials.

In contrast to this finding we note that a cluster of 25 spheres reflects the influence of the sphere material (see Fig. 9). On the one hand we do not see any difference at low frequencies ($f_d \leqslant 2.5$ Hz) but on the other hand f_s changes dramatically at high driving frequencies: Bronze and brass only show a slight difference while rough and polished glass deviate systematically at higher frequencies. PUR has the most noticeable effect and only tends to slow down at $f_d = 4.5$ Hz. Unfortunately limitations in the apparatus do not allow us to perform measurements at higher frequencies. Comparing the results of Fig. 8 and Fig. 9 shows that the differences in the dynamics of the cluster for different materials are not governed by sphere-container interactions; here the sphere-sphere interactions influence the behavior for different materials.

Impact experiments [21] show that the restitution coefficient, which indicates how much energy is dissipated during a binary collision, is velocity dependent. For example, the restitution coefficients of bronze and brass decrease with increasing impact velocity. Because it is obvious that we get higher sphere velocities at higher driving frequencies it is natural that the cluster has to slow down when the restitution coefficient is smaller. In the case of bronze and brass this picture is in agreement with the findings of Goldsmith [21]. Because we do not know the velocity dependence of the restitution coefficient of our five different materials we only

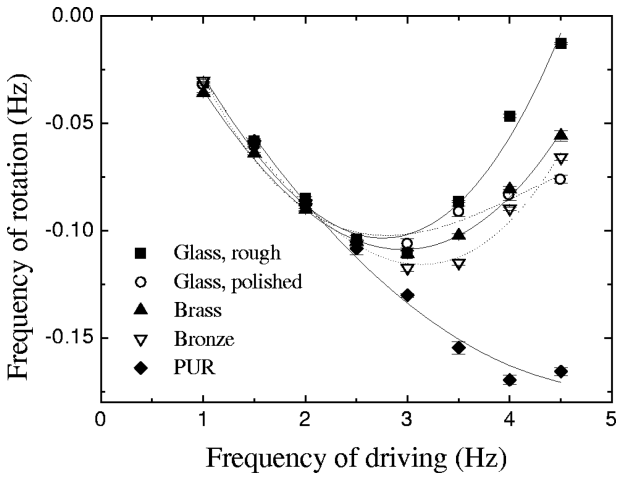

FIG. 9. Dependence of the frequency of rotation on the driving frequency for different material (number of spheres: 25; channel width: 10.5 mm). All curves have parabolic shapes except for polished glass where a cubic fit is more reasonable.

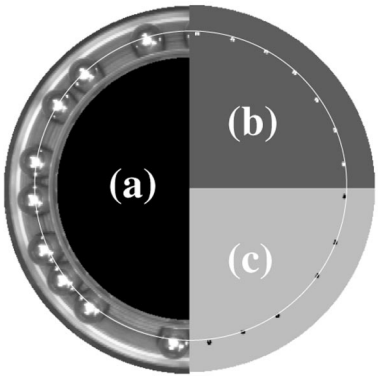

FIG. 10. Stages for taking space-time plots: (a) shows a real image with the top view of the experiment. Spheres appear with a light spot in the center. (b) shows a real image with reduced aperture. The white line crossing the white spots is digitized and appears as the space coordinate in Fig. 11. (c) Inverted image of (b).

can speculate on the influence of different materials. Again further examinations are encouraged. Our apparatus might also be suitable to uncover influences of material parameters because microscopic behavior like the dynamics of a binary collision is transferred onto a mesoscopic scale where it gives rise to a global dynamical behavior, the rotation of the cluster.

4. Visualization of particle dynamics

In an alternative experimental approach to understand the basic mechanism of the process we visualize the trajectories of the particles. Figure 10 shows the different steps of our procedure. The experimental conditions are chosen for comparison with the phase diagram of Fig. 2, i.e., $f_d = 2.5$ Hz, $w = 10.5$ mm and bronze as bead material. Figure 10(a) gives a real image of the top view of the setup taken by the CCD camera. Due to the lighting of the annular lamp (see Fig. 1) the center of mass of single spheres appear as bright spots. We now lower the aperture of the camera because we are only interested in the center of mass of the spheres. This also enhances the contrast of the images [see Fig. 10(b)]. The center of the spheres now appear as tiny light spots. Because it is more convenient to look at black spots on a light background we invert the image and show its negative [see Fig. 10(c)]. Next, we only take shots of the middle of the annular channel. In Fig. 10 these points appear as a thin white circle that crosses the center of mass of the spheres. The circle is divided counterclockwise into 512 points and plotted as a space time plot in Fig. 11. We take images every 20 ms. Because of the clearance of the spheres with respect to the channel width we unfocus the camera. Hence, the center of the spheres appears broader and are available at every step of the visualization process. This has the advantage that we do not get voids in our space time plots when the center of the particles are not exactly in the middle of the channel and the spots get lost.

In Fig. 11 we present twelve space-time evolutions for different numbers of spheres. The number in the upper left corner of each image denotes the number of particles in the annulus. An inlet in the upper right corner shows a magnified section of the space time plot. This gives a more detailed view of the particle dynamics in addition to the global behavior of the total image. We plot the 512 points of our digitized circle horizontally. This means that left and right sides yield periodic boundaries. The vertical coordinate gives the time. We show 512 lines that represent an observation time T of 10.24 s. Time starts at the bottom of each image and continues to the top.

For $N = 10$ we see the dynamical behavior of spheres in the no collision zone. On each horizontal line the center of mass of each bead appears as a black spot. As time progresses the spheres shift to the right. Despite this global translation, a single sphere oscillates back and forward as time proceeds. The forward motion is larger than the back motion that results in a positive translatory movement. This behavior is found for every particle. By looking at the global behavior it is also clear that the spheres do not have the same translatory velocities. There are regions where the packing density is higher and the spheres slow down. This might be caused either by inhomogeneities of the channel that can be noticed in space-time plots with an extended time coordinate or by single binary collisions, which reduce the speed of the particles even though collisions are rare at this stage. As the number of particles increases the probability for collisions is enhanced. Note that the black lines of the trajectories do not touch because they represent the center of mass of the spheres. A collision occurs when the distance between two black spots on a horizontal line equals one particle diameter. Near the critical point where the sense of rotation changes we see large scale fluctuations of the oscillation amplitude (see $N = 21$ and 22 in Fig. 11). Here we also see voids where the packing density is low and areas where the packing density is high. For $N \geqslant 22$ strength of the forward motion vanishes, the cluster is in the reptation mode and moves in the negative direction. It is also observed that the space time plots have an ordered structure for large N whereas the degree of order is less at the critical point due to fluctuations.

In Sec. II B 1 we pointed out that we observe longitudinal density waves by visual inspection of our setup. These LDWs are also found in the presented space time plots. In Fig. 11, e.g., for $N = 25$ we see the collision point where one sphere moves back and then suddenly collides with the sphere on the left side which itself moves in positive direction. As a result the back moving sphere changes its direction and collides with its back moving neighbor on the right. Hence, we get a new collision point. As time goes on this point shifts in positive direction. Connecting all the collision events we get a line that is tilted with respect to the horizontal (see $N = 25$ in Fig. 11). For $N = 23$ we also observe this line, but it is obvious that the wave breaks up due to voids.

In summary, by visualizing particle trajectories in our annulus we find the following dynamical features of our system: First, a single particle has a slow positive drift and in addition shows a fast oscillation reflecting the driving frequency. This is in good agreement with a theoretical model that is presented in the next chapter and uncovers the basic mechanism of the observed phenomenon. Second, near the critical point long scale fluctuations are found. For high packing densities the space time plots display an ordered structure. Finally we showed the existence of LDWs.

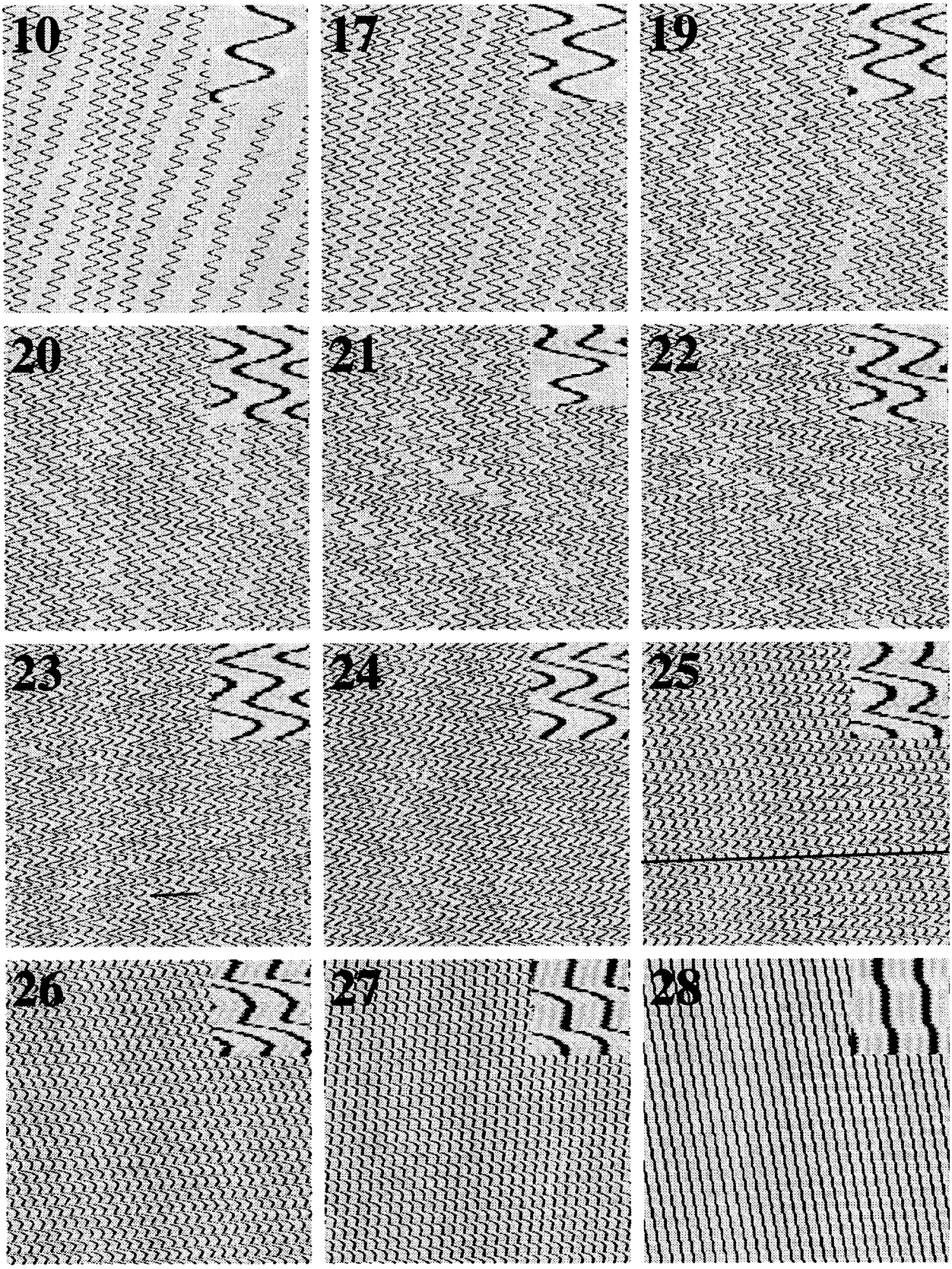

FIG. 11. Space-time evolution of sphere traces. The centers of mass of the spheres appear black (material: bronze; channel width: 10.5 mm; driving frequency: 2.5 Hz). The horizontal axes are the space coordinates (0 to 2π) while the vertical axes show the time (0 to 10.24 s). The number in the upper left corner denotes the number of spheres. A magnified section can be seen in the upper right corner. For $N=23$ and $N=25$ a straight line indicates a longitudinal density wave.

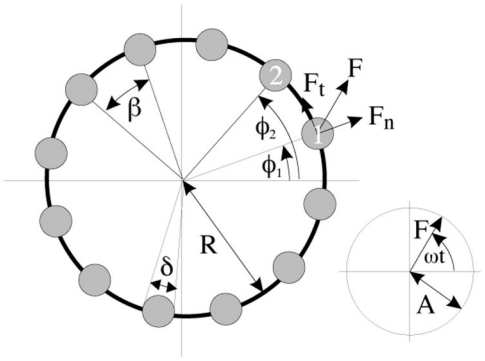

FIG. 12. Model arrangement.

III. THEORY

A. Dynamics of a single sphere

For a theoretical discussion of the observed phenomena we start with the analytical description of the behavior of a single bead in a swirled annulus. Assuming that the channel width coincides with the diameter of the bead we arrive at a one-dimensional model in which the position of the sphere is specified by the angle ϕ (see Fig. 12). The equation of motion is

$$m\ddot{\phi}+\Gamma\dot{\phi}+\frac{A\omega^2 m}{R}\sin(\phi-\omega t)=0, \tag{6}$$

where m denotes the mass of the bead, R the distance of its center from the center of the annulus, and A and ω amplitude and frequency of the swirling motion, respectively. We have assumed a simple phenomenological friction law with constant Γ to treat the complicated process of stick-slip motion on the surface of the container and the interaction with the boundaries. Although other laws might be more realistic for granular material we will stick to this simple form in the present discussion.

Rescaling time by $t\rightarrow\omega t$ we find the dimensionless form of Eq. (6)

$$\ddot{\phi}+\eta\dot{\phi}+\varepsilon\sin(\phi-t)=0, \tag{7}$$

where

$$\eta=\frac{\Gamma}{m\omega} \quad \text{and} \quad \varepsilon=\frac{A}{R}. \tag{8}$$

There are two qualitatively different solutions to this equation that can be most easily distinguished by transforming into the comoving coordinate system via $\psi=\phi-t$. We then get

$$\ddot{\psi}+\eta\dot{\psi}=-\varepsilon\sin\psi-\eta=-\frac{\partial}{\partial\psi}(\eta\psi-\varepsilon\cos\psi) \tag{9}$$

and ψ simply performs a damped motion in a tilted cosine potential (see Fig. 13). It is clear that for $\varepsilon/\eta>1$, i.e., if $Am\omega/(\Gamma R)>1$, there are stationary solutions of Eq. (9) in the minima of the potential corresponding to *revolutions of the bead with the frequency of the external driving*. Note that this condition is always fulfilled for $\Gamma\rightarrow 0$.

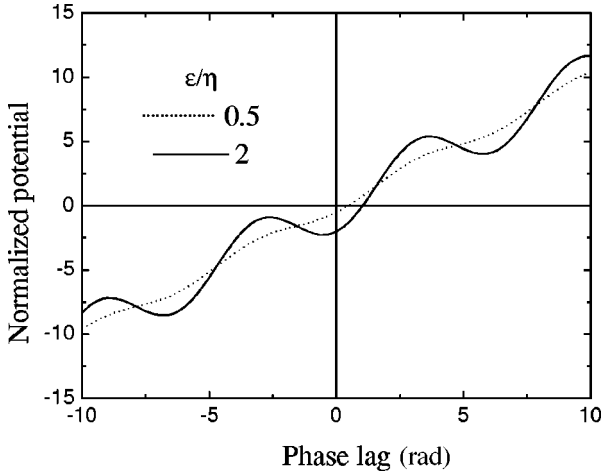

FIG. 13. Normalized potential $V/\eta=\psi-\epsilon/\eta\cos\psi$.

On the other hand if $\varepsilon/\eta<1$ no stationary solutions of Eq. (9) exist and the bead permanently lags behind the external swirling. It is this regime that is relevant to the experiments in which $\varepsilon\simeq 0.2$ and a single bead shows a slow drift superimposed by small oscillations with the external frequency ω. To account for this motion we split $\phi(t)$ into a slow part $\varphi(t)$ and a fast oscillating part with small amplitude $\delta\varphi(t)$:

$$\phi(t)=\varphi(t)+\delta\varphi(t) \tag{10}$$

and try to find an equation of motion for $\varphi(t)$ by averaging over $\delta\varphi$ [22].

Using Eq. (10) in Eq. (7) we get

$$\begin{aligned}\ddot{\varphi}+\delta\ddot{\varphi}+\eta\dot{\varphi}+\eta\delta\dot{\varphi}&=-\varepsilon\sin(\varphi+\delta\varphi-t)\\&\simeq-\varepsilon\sin(\varphi-t)+\varepsilon\cos(\varphi-t)\delta\varphi.\end{aligned} \tag{11}$$

The slow and the fast part of ϕ must fulfill this equation separately. For the fast part we find

$$\delta\ddot{\varphi}+\eta\delta\dot{\varphi}=-\varepsilon\sin(\varphi-t) \tag{12}$$

$$\delta\varphi=-\varepsilon\int_0^t dt' e^{-\eta(t-t')}\cos(\varphi-t'), \tag{13}$$

where we have neglected the term involving both ε and $\delta\varphi$ and assumed that φ is constant at the scale of $\delta\varphi$. Using this result in Eq. (11) and averaging over one period of the external forcing we arrive at

$$\ddot{\varphi}+\eta\dot{\varphi}=\frac{\varepsilon^2\eta}{2(1+\eta^2)}-\frac{\varepsilon^2(1-e^{-2\pi\eta})}{2\pi(1+\eta^2)^2}[(1+\eta^2)\cos^2\varphi-1]. \tag{14}$$

For not too small η the second term is negligible and we simply get

$$\ddot{\varphi}+\eta\dot{\varphi}=\frac{\varepsilon^2\eta}{2(1+\eta^2)} \tag{15}$$

yielding

$$\varphi(t)=\frac{\varepsilon^2}{2(1+\eta^2)}t+\text{const.} \tag{16}$$

This equation could also be derived from Eq. (7) by neglecting the inertial term. It describes the slow average drift of the bead around the annulus induced by the swirling motion as observed in the experiments and serves to determine η. In the following sections we want to refer to an experimental sample (see Fig. 2). Thus, ϵ is fixed by the experimental setup to 0.21 and the drift of a single bead is given by 0.015 in terms of f_d. Hence we get $\eta=0.7$.

B. Free path restriction

By looking at the dynamics of a single sphere we showed that the motion of a swirling table stimulates a bead to drift in one direction accompanied by a fast back and forward oscillation. In a second approach it is interesting to ask: What will happen if we consider two or even more spheres? Is there a condition for which they collide? It is obvious that increasing the packing density of the system decreases the free path β of the spheres, where $\beta=2\pi/N$ (see Fig. 12). If $\beta-\delta$ is of the order of the mean oscillation amplitude of a single sphere that can be expressed by an angle α one can expect that two neighboring spheres will collide. Here δ represents the sphere diameter in angular units. In the experiment δ is always 0.22. Under the conditions that result in the phase diagram seen in Fig. 2 the positive amplitude a is 6.5 mm, which gives $\alpha=0.15$. Hence we get a critical number N_c of 17 spheres for our above-mentioned experimental conditions. For $N<17$ two neighboring spheres will not touch whereas they will collide if N exceeds this critical number. N_c is in good agreement with experimental findings. We found that for $N>16$ there will be single collisions that slow down the rotation period of the cluster.

Adding two assumptions to the idea that collisions occur when individual oscillations become restricted leads to a more sophisticated model: First we suppose that the spheres are distributed homogeneously throughout the annulus as in Fig. 12. Second we simplify the dynamics of a single sphere by only allowing a constant drift ν superimposed on a sinusoidal oscillation:

$$\phi_n=\alpha\sin(\omega t-\phi_{n0})+(n-1)\beta+\nu t, \tag{17}$$

where n denotes the bead in the annulus, $\phi_{n0}=\phi_n-\phi_0$, $\phi_n=\phi_1+(n-1)\beta$, and ϕ_0 is a phase delay.

While this gives an oversimplified picture of the motion of a single sphere we believe that it is sufficient to track down an initial collision model involving many spheres. However, we only have to consider two spheres (e.g., sphere 1 and sphere 2 in Fig. 12).

Thus, for $n=1$ we get

$$\phi_1=\alpha\sin(\omega t)+\nu t \tag{18}$$

and for sphere 2:

$$\phi_2=\alpha\sin(\omega t-\beta)+\beta+\nu t. \tag{19}$$

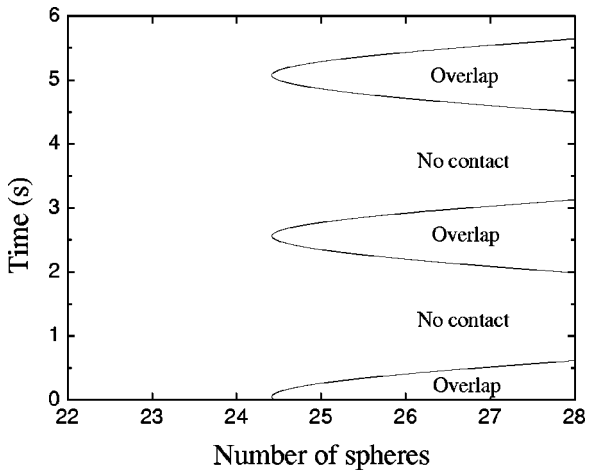

FIG. 14. Visualization of the free path restriction. The solid line refers to the point where the spheres touch. In between there are zones of no contact and zones where the spheres theoretically overlap. Parameters are chosen to represent the conditions similar to those of Fig. 2.

For simplicity we suppose that $\phi_0=0$, i.e., we skip the phase delay. Moreover, $\phi_2=\phi_1+\beta$ with $\phi_1=0$ for $t=0$. Finally, we have to define a condition where the two spheres initially touch:

$$\phi_1-\phi_2\leqslant\delta. \tag{20}$$

With Eq. (18) and Eq. (19) we obtain

$$\cos(\omega t-\beta/2)\sin(\beta/2)\geqslant\frac{\beta-\delta}{2\alpha}. \tag{21}$$

Because $\sin(\beta/2)$ and $(\beta-\delta)/(2\alpha)$ always exceed 0 and $\cos(\omega t-\beta/2)$ can be negative, it is obvious that our initial condition [Eq. (20)] is restricted with respect to the phase of motion ωt. This means that we do not get a solution for $\pi/2+\beta/2<\omega t<3\pi/2+\beta/2$. For $-\pi/2+\beta/2<\omega t<\pi/2+\beta/2$ two solutions can be obtained by solving Eq. (21) for t:

(i) $(\pi/\omega)(1/N+k)<t<(\pi/\omega)(1/N+k+1/2)$:

$$t\leqslant-\frac{1}{\omega}\arccos\left[\left(\frac{\pi}{N\alpha}-\frac{\delta}{2\alpha}\right)\frac{1}{\sin(\pi/N)}\right]+\frac{\pi}{\omega N}+\frac{2\pi k}{\omega} \tag{22}$$

and

(ii) $(\pi/\omega)(1/N+k-1/2)<t<(\pi/\omega)(1/N+k)$:

$$t\geqslant-\frac{1}{\omega}\arccos\left[\left(\frac{\pi}{N\alpha}-\frac{\delta}{2\alpha}\right)\frac{1}{\sin(\pi/N)}\right]+\frac{\pi}{\omega N}+\frac{2\pi k}{\omega}. \tag{23}$$

Here, for convenience, β is expressed in terms of the number of particles N and $k=0,2,4,\ldots$.

In Fig. 14, we plot Eq. (22) and Eq. (23) as a function of particle number N for our experimental sample. It indicates that below a critical number N_c, which is about 24.5 there exists no solution, i.e., the spheres do not collide. Increasing the packing density has the effect that our initial condition

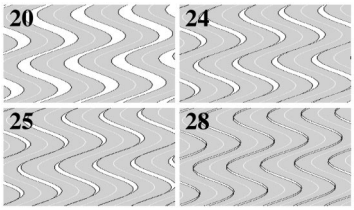

FIG. 15. Simulation of the space-time evolution under sample conditions. The horizontal axes show the space coordinate (only a part of the annulus is shown). Time is on the vertical axes (two oscillations are seen). The spheres appear in gray, centers of mass in white, and borders in black. The number of spheres in the annulus is found in the upper left corner.

[Eq. (20)] becomes valid and the beads touch and even overlap theoretically. Note that in the experiment an overlap is not possible; the spheres either separate or stick together for a certain period. For $N=25$, 26, 27, and 28 we get phases where the spheres first touch, overlap and then again separate. This behavior is periodic in time. To support this we simulate the time evolution of the traces of some spheres for different particle numbers (see Fig. 15). For $N=20$ the trajectories are not disturbed whereas they come close when the particle number is increased to 24. In the case of $N=25$ we see that the spheres collide and even overlap slightly. For 28 particles this tendency is enhanced. Note that collision and overlap only take place during forward movement of the spheres. In contrast, the spheres are separated while moving back. What happens when the spheres touch or overlap? In reality the spheres can only collide. This means that due to the inelastic character of the material energy will be dissipated and therefore the forward motion has to slow down. Moreover it is worthwhile to consider that the spheres might stick together during the phase of theoretical overlap. Because the spheres rotate in the same sense there is shear at the contact point. This means that even more energy is dissipated. Thus the idea is supported that the forward motion will be depressed due to collisions and tangential shear. In the extreme case the two spheres will stop moving in the positive direction and only move back. These considerations are confirmed by looking at the experimental space-time plots presented in Fig. 11. For $N=28$ it is clear that the beads do not move in the positive direction at all. However, they separate for some time during the phase of back motion so they get the chance to slide or roll back.

In our opinion the idea of a free path restriction covers the main mechanism of the effect that swirling granular matter in an annular channel results in a change of the sense of rotation when the number of particles is increased: At low packing densities single trajectories of the spheres are not disturbed, the distance traveled in the positive direction is larger than in the negative one. This gives a constant drift. When the particle number is increased the spheres touch during forward motion and dissipate energy. This restricts forward motion. At the critical point the forward and back movements equalize and the spheres just oscillate with no drift although large fluctuations of the oscillation amplitude are observed (see, e.g., $N=21$ in Fig. 11). For high packing densities dissipation is so high that the back motion predominates.

Why do we not see a change of the sense of rotation between $N=24$ and 25 in the experiment? In our opinion this is due to the fact that in our model we suppose a constant drift for each particle and a homogeneous distribution. Under experimental conditions this assumption breaks down and the critical point is shifted to smaller particle numbers.

C. Many particle simulation

To support the idea that energy dissipation by binary collisions is responsible for the change of the rotation sense in the annular channel we simulate Eq. (6) for many particles [23]. The computational procedure consists of two different steps: First we adjust our numerical system by looking at the dynamics of a single sphere. In Eq. (6) we got two different parameters η and ϵ, which govern the dynamics. Because we again want to refer to our experimental sample (see Fig. 2), ϵ is fixed by the experimental setup to 0.21. η was determined by Eq. (16) to be 0.7. Second we investigate the behavior of many particles. We initialize our system by choosing random values for space coordinates and velocity. We solve the basic equation for the first particle and ask for its new position after a certain time step dt. Next we look at whether it touches one of its neighboring particles. In the case that there is no collision event we proceed to the next particle. When there is a collision between two spheres we calculate their new velocities v_1' and v_2'. Two different models were used to simulate the collision process. In the first model [11] energy dissipation is introduced by reducing the relative motion of both particles:

$$v_2'-v_1'=-\nu(v_2-v_1), \tag{24}$$

where ν is the coefficient of restitution that for simplicity is assumed to be independent of the incident velocity. Combined with the conservation of momentum we hence get

$$\begin{pmatrix} v_1' \\ v_2' \end{pmatrix} = \begin{pmatrix} (1-\nu)/2 & (1+\nu)/2 \\ (1+\nu)/2 & (1-\nu)/2 \end{pmatrix} \begin{pmatrix} v_1 \\ v_2 \end{pmatrix}. \tag{25}$$

Figure 16(a) compares the numerical results with experimental findings. Here we vary the restitution coefficient to show its influence on many particle dynamics. We let the spheres relax during a period of $t=20/f_d$. Next the velocities of all spheres are averaged over $t=100/f_d$. This gives reproducible values. The system is not sensitive to dt, which we choose to be 0.001 in units of $1/f_d$. It is obvious that the revolution frequency of the beads in the no collision zone is independent of ν. In contradiction to the experiment we find that for $N>20$ the velocities of the cluster first increase and then decrease for large packing densities. Finally, when the ring is almost filled with particles, the rotation sense changes. Varying the coefficient of restitution only shows a slight influence on the behavior. Even in the case of completely inelastic collisions, where $\nu=0$, we are not able to reproduce the experimental results.

Due to this obvious discrepancy we tested a second model where we reduce the transmitted momentum during a binary collision:

$$v_2'+v_1'=\mu(v_2+v_1), \tag{26}$$

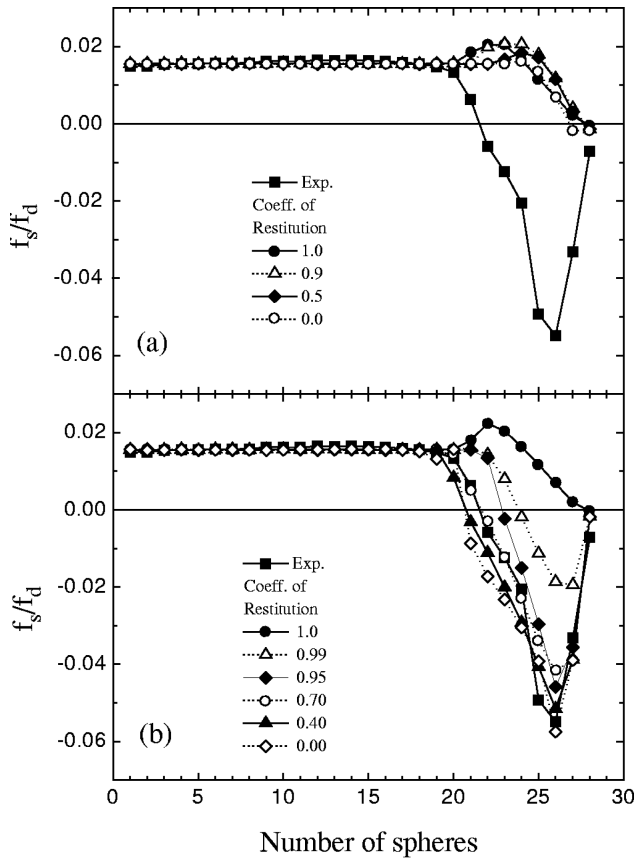

FIG. 16. Comparison of experimental results with numerical simulations of many particles with respect to the coefficient of restitution. Parameters are chosen to match with conditions of those in Fig. 2. In (a) we assume a model where the coefficient of restitution reduces the relative velocity of two colliding spheres whereas in (b) we assume a model in which the absolute value of the particle velocity is reduced.

where μ is a number between 0 and 1 that gives the amount of momentum that is conserved during a binary collision. The conservation of momentum is violated in two ways. First, sphere collisions are not central due to the clearance of the spheres in the annular channel. Thus the contact between the particles is also mediated by contact with the walls of the channel. Second tangential friction at the contact point plays a significant role during the collision process. Combining Eq. (24) and Eq. (26) and with $\mu=\nu$ we obtain

$$\begin{pmatrix} v_1' \\ v_2' \end{pmatrix} = \begin{pmatrix} 0 & \nu \\ \nu & 0 \end{pmatrix} \begin{pmatrix} v_1 \\ v_2 \end{pmatrix}. \tag{27}$$

Thus the rather complicated collision process is expressed by an effective coefficient of restitution, which simply reduces the normal velocity of both spheres.

In Fig. 16(b) we again compare our numerical findings with the experimental values. For $\nu=1$ we do not get an agreement with our experiment. In this case only for $N=28$ a change in the sense of rotation of the cluster is found. This behavior changes dramatically for $\nu=0.95$ where we already approach the empirical findings. Using lower coefficients of restitution does not alter the global behavior. For $\nu=0.7$ we get a good agreement in the transition zone, only the points for $N>26$ do not match exactly.

Comparing the numerical results of both models we conclude that a model that only describes energy dissipation by central collisions in addition to conservation of momentum does not reflect the experimental situation. We believe that due to the rotational motion of the spheres and noncentral collisions leading to wall contact momentum gets lost during each collision process. Improved collision models that treat the spheres as rotating three-dimensional objects and include a coefficient of rotational restitution and a coefficient of sliding friction as demonstrated, e.g., in Ref. [24] could be used to confirm this interpretation.

IV. CONCLUSIONS

The phenomenon that a layer of granular material changes its sense of rotation while swirled in a container was investigated in an annular channel. This reduced system uncovers the basic mechanism of the effect. It is also suited to study collision dynamics of granular columns. It was found that the global behavior is not changed by the width of the channel but that it shows influences of different possible packing structures. The critical point where there is a transition from rotation to reptation mode does not depend only on the number of particles but also on the driving frequency. At high frequencies we showed that the material parameters become significant. By visualizing the particle trajectories we hinted at how to model the dynamics of a single sphere. Moreover long scale fluctuations at the critical point and a transition to an ordered state at high packing densities were presented. Our simple one-dimensional model is in good agreement with our experimental findings. The dynamics of a single particle can be related to a friction coefficient and the ratio of shaking amplitude to the radius of the channel. The typical experimental behavior, which consists of a slow drift and a fast oscillation of the bead, was confirmed. Finally, by introducing the idea of a free path restriction and by simulating our basic equation for many particles we tracked down the mechanism of the observed effect: Binary collisions only occur when the packing density exceeds a critical number and when the spheres swing in the positive direction. In this case the forward motion is suppressed by energy dissipation. At high packing densities the back swing predominates and the whole cluster turns the other way around.

ACKNOWLEDGMENTS

It is a pleasure to thank J. Anine, B. Eckhardt, K. Kuehn, S. Rudroff, W. van Saarloos, M. Schröter, and G. Straßburger for valuable discussions. We owe much to T. Bock, H. Brunn, and T.-M. John for performing surface roughness measurements. This project was supported by the Deutsche Forschungsgemeinschaft through Grant No. Re 588/11-1, 2.

[1] H. M. Jaeger and S. R. Nagel, Rev. Mod. Phys. **68**, 1259 (1996).
[2] H. J. Herrmann, in *3rd Granada Lectures in Computational Physics*, edited by P. L. Garrido and J. Marro (Springer, Heidelberg, 1995), pp. 67–114.
[3] B. Miller, C. O'Hern, and R. Behringer, Phys. Rev. Lett. **77**, 3110 (1996).
[4] N. Sela and I. Goldhirsch, Phys. Fluids **7**, 507 (1995).
[5] P. B. Umbanhowar, F. Melo, and H. L. Swinney, Nature (London) **382**, 793 (1996).
[6] T. Zhou and L. P. Kadanoff, Phys. Rev. E **54**, 623 (1996).
[7] M. A. Scherer, V. Buchholtz, T. Pöschel, and I. Rehberg, Phys. Rev. E **54**, R4560 (1996).
[8] G. Giese and A. Zippelius, Phys. Rev. E **54**, 4828 (1996).
[9] N. V. Brilliantov, F. Spahn, J.-M. Hertzsch, and T. Pöschel, Phys. Rev. E **53**, 5382 (1996).
[10] S. McNamara and W. R. Young, Phys. Rev. E **53**, 5089 (1996).
[11] E. Grossman and M. Mungan, Phys. Rev. E **53**, 6435 (1996).
[12] N. Schörghofer and T. Zhou, Phys. Rev. E **54**, 5511 (1996).
[13] A. Kudrolli, M. Wolpert, and J. P. Gollub, Phys. Rev. Lett. **78**, 1383 (1997).
[14] F. Radjai and S. Roux, Phys. Rev. E **51**, 6177 (1995).
[15] D. R. M. Williams and F. C. MacKintosh, Phys. Rev. E **54**, R9 (1996).
[16] A. N. Lazaridi and V. F. Nesterenko, J. Appl. Mech. Tech. Phys. **26**, 405 (1985).
[17] F. Radjai, M. Jean, J.-J. Moreau, and S. Roux, Phys. Rev. Lett. **77**, 274 (1996).
[18] A. Sommerfeld, *Vorlesungen über Theoretische Physik I - Mechanik* (Akademische Verlagsgesellschaft Geest & Portig, Leipzig, 1954), Sec. 27.
[19] T. G. Drake, J. Fluid Mech. **225**, 1991 (1991).
[20] W. Greiner, *Mechanik Teil 2* (Harri Deutsch, Thun, 1989), p. 196.
[21] W. Goldsmith, *Impact* (Edward Arnold Ltd., London, 1960), p. 258.
[22] L. D. Landau and E. M. Lifshitz, *Lehrbuch der Theoretischen Physik I - Mechanik* (Akademie, Berlin, 1990), Sec. 30.
[23] An interactive Java simulation of the numerical system can be found under URL http://comserv.urz.uni-magdeburg.de/~anp/safe/swirlsim/swirlsim.html at World Wide Web. Various parameters like coefficient of restitution or number of spheres can be varied.
[24] O. R. Walton, in *Particulate Two-Phase Flow*, edited by M. C. Roco (Butterworth-Heinemann, Boston, 1993), p. 884.